Pre-print submitted version

Phosphine Oxide Derivative as a Passivating Agent to Enhance the Performance of Perovskite Solar Cells

Albertus Adrian Sutanto, Cansu Igci, Hobeom Kim,* Hiroyuki Kanda, Naoyuki Shibayama, Mounir Mensi, Valentin I. E. Queloz, Cristina Momblona, Hyung Joong Yun, Henk J. Bolink, Aron J. Huckaba, and Mohammad Khaja Nazeeruddin

ABSTRACT: Defects of metal-halide perovskites detrimentally influence the optoelectronic properties of the thin film and, ultimately, the photovoltaic performance of perovskite solar cells (PSCs). Especially, defect-mediated nonradiative recombination that occurs at the perovskite interface significantly limits the power conversion efficiency (PCE) of PSCs. In this regard, interfacial engineering or surface treatment of perovskites has become a viable strategy for reducing the density of surface defects, thereby improving the PCE of PSCs. Here, an organic molecule, tris(5-((tetrahydro-2H-pyran-2-yl)oxy)pentyl)phosphine oxide (THPPO), is synthesized and introduced as a defect passivation agent in PSCs. The P□O terminal group of THPPO, a Lewis base, can passivate perovskite surface defects such as undercoordinated Pb2+. Consequently, improvement of PCEs from 19.87 to 20.70% and from 5.84 to 13.31% are achieved in n−i−p PSCs and hole-transporting layer (HTL)-free PSCs, respectively.

KEYWORDS: perovskite solar cells, defect passivation, surface passivation, HTL-free, phosphine oxide, Lewis base.

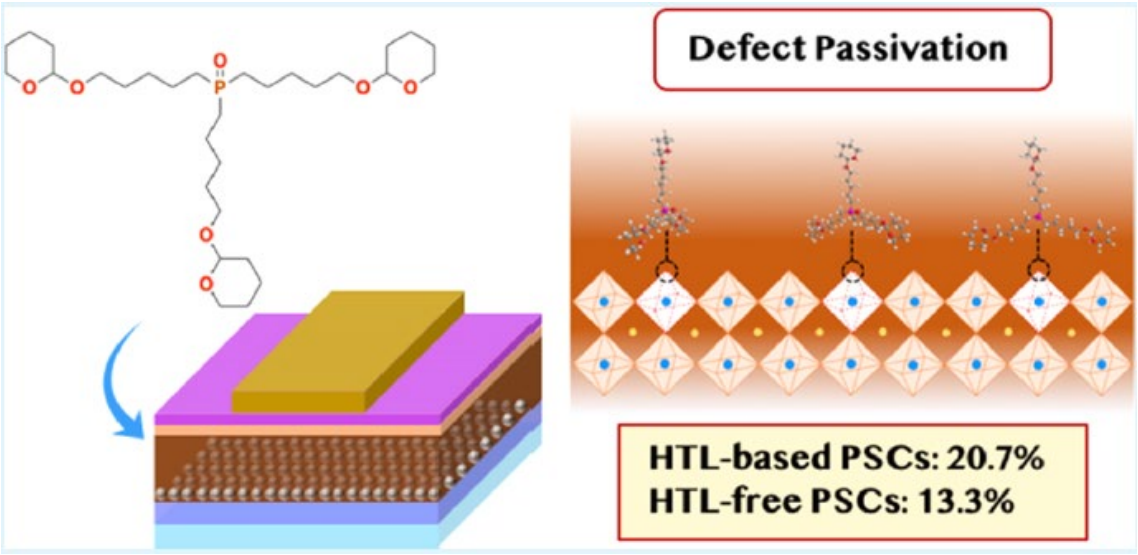

INTRODUCTION

Perovskite solar cells (PSCs) have rapidly advanced and recently achieved 25.5% power conversion efficiency (PCE)

since the first report with a PCE of 3.8% in 2009.1,2 The great evolution of PSCs is basically attributed to the outstanding optoelectronic properties of the light absorber, such as broad optical absorption,3,4 tunable band gap,5,6 long charge-carrier diffusion length,7−9 and ambipolar p- and n-type conduction.

10,11 Also, extensive research on the structural design of devices, interfacial layer engineering, and device physics under operating conditions has also contributed to the considerable development of PSCs.12 Nevertheless, perovskites defects continue to be treated as they detrimentally influence the photophysical and photoelectrical properties of films and devices. Defects can induce the formation of trap states in the perovskite and at the interface with the adjacent layer, which can cause undesirable nonradiative recombination.13−20 Undercoordinated Pb^{2+} can especially influence charge-carrier dynamics leading to the loss of charge carriers, thereby degrading the photovoltaic performance.21−23 Therefore, it is necessary to design and develop defect passivation strategies to improve device performance.

To date, various defect passivation strategies in PSCs have been reported using inorganic24−26 and organic molecules27−30 and polymers,21,31,32 also through additive engineering,33,34 grain-boundary engineering,35 and multidimensional engineering, 36−39 which can result in reduced nonradiative charge recombination, efficient charge collection, and thereby improving device performance.21,24−39 One of the effects that defect passivation can exert is to reduce the undercoordinated Pb^{2+} in the perovskite by taking advantage of the Lewis base materials that have validated the improvement of carrier dynamics and device performance.40−46 Among the Lewis base materials, molecules including phosphine oxide such as tri-noctylphosphine oxide (TOPO),42,47−50 triphenylphosphineoxide (TPPO),45 and tetraisopropyl

methylenediphosphonate (TMPP)45 have been regarded as promising passivation agents due to their electron-donating ability.

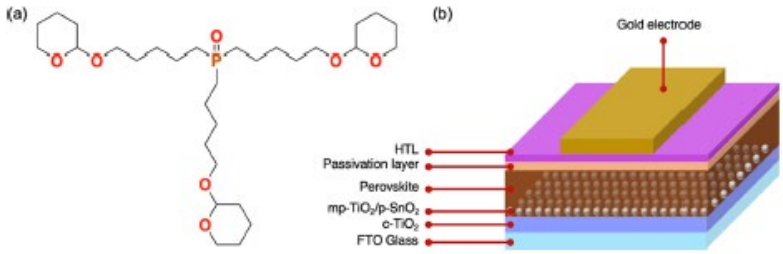

Figure 1. (a) Molecular structure of THPPO and (b) device structure of n–i–p PSCs employing fluorine-doped tin oxide (FTO), compact TiO2 (c-TiO2), mesoporous TiO2 (mp-TiO2), SnO2, perovskite, THPPO as a passivation layer, HTL, and gold electrode.

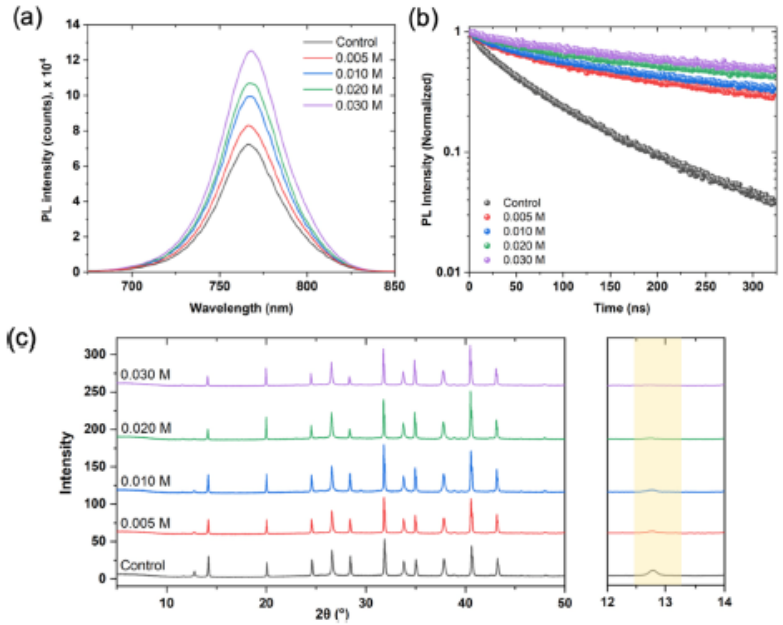

Figure 2. (a) Steady-state PL spectra (λexc = 550 nm), (b) time-resolved PL spectra (λexc = 480 nm), and (c) XRD patterns of control perovskite film and passivated films with various concentrations of THPPO.

In this study, we synthesized a new Lewis base organic molecule containing a phosphine oxide group ((tetrahydro-2H-pyran-2-yl)oxy)pentyl phosphine oxide (THPPO) as a passivating agent on top of a perovskite layer (Figure 1a). The P□O group of THPPO led to the formation of a chemical bond with the undercoordinated Pb2+ on the surface of the perovskite. The perovskite film treated with THPPO showed reduced nonradiative carrier recombination and an improved PCE of PSCs. We incorporated THPPO in two different types of devices: one with a n–i–p configuration (Figure 1b) and the other with a hole-transporting layer (HTL)-free configuration for the development of simplified and cost-effective PSCs. The introduction of THPPO led to an improvement in PCE from 19.87 to 20.70% for the n–i–p devices and 5.84 to 13.31% for the HTL-free devices.

RESULTS AND DISCUSSION

In the molecular design of THPPO, the phosphine oxide group that provides a Lewis base was chosen as an active passivation agent for the perovskites. It was functionalized with a fivecarbon alkyl substituent chain to make it soluble in common organic solvents. The tetrahydropyranyl ether unit was combined with the ether group as effective anchors at the interface between perovskite and HTL.51 The general synthetic scheme and the detailed synthetic procedure of THPPO are presented in Scheme S1 and the Supporting Information. The synthesis of THPPO began with a carboxylic acid reduction reaction of the commercially available 5-bromopentanoic acid by the borane−tetrahydrofuran complex to the corresponding primary alcohol.52 The obtained 5-bromopentan-1-ol was then attached to tetrahydropyran (THP) group in the presence of ptoluenesulfonic acid in dichloromethane to attain tetrahydropyranyl ether functional group.53 As a last step, 2-((5- bromopentyl)oxy)tetrahydro-2H-pyran with magnesium formed a Grignard reagent, which reacted with phosphorous trichloride to furnish an alkyl-phosphine intermediate product.

Then, the intermediate product was oxidized with hydrogen peroxide in dichloromethane in high yield to obtain a novel passivation molecule THPPO.54,55 Purification of the final compound was performed by column chromatography without the need for high-pressure vacuum distillation. The synthesized product chemical structure was verified by 1H, 13C, and 31P nuclear magnetic resonance (NMR) spectroscopy and mass spectroscopy (Figures S1 and S2). THPPO is soluble in common organic solvents such as tetrahydrofuran (THF), chloroform, toluene, and chlorobenzene, typically used for the deposition of a passivation layer in the PSCs.

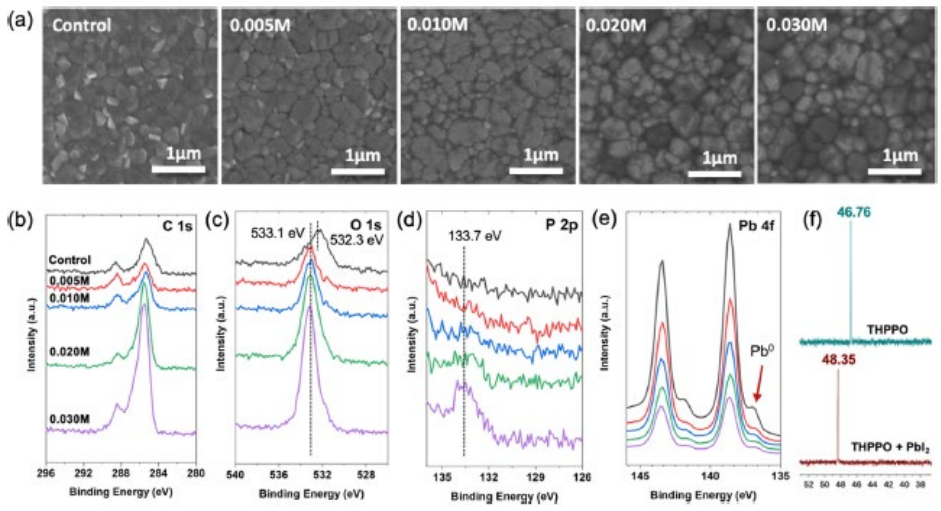

Figure 3. (a) SEM images: surface morphology of control perovskite film and films with various concentrations of THPPO. Core-level XPS spectra of (b) C 1s, (c) O 1s, (d) P 2p, and (e) Pb 4f of control perovskite film and films with various concentrations of THPPO. (f) 31P NMR spectra of 0.01 mmol THPPO and THPPO mixed with 0.01 mmol PbI2 in dimethyl sulfoxide (DMSO)-d6.

We deposited the THPPO solution dissolved in chlorobenzene with various concentrations (0.005, 0.010, 0.020, and 0.030 M) on top of a triple-cation-based perovskite layer [(FAPbI3)0.87(MAPbBr3)0.13]0.92(CsPbI3)0.08. Figure 2a shows the

steady-state photoluminescence (PL) spectra of the control and THPPO-treated perovskite thin films. The films were excited with 550 nm light from the top side of the film. The emission spectra of all of the films show a peak at 767 nm regardless of the concentration of THPPO while the PL intensity was improved by increasing the concentration of THPPO. The absorption spectra of the films did not show any new absorption peak and a noticeable shift of the band edge at 780 nm (Figure S3). The improvement of the PL intensity can be attributed to the passivation effect of THPPO, which can lead to a reduction of the density of trap states in the perovskite with enhanced radiative recombination. Meanwhile, the unchanged position of the PL emission peak and the absorption onset implies that the deposition of THPPO did not degrade or modify the crystal structure of the underlying perovskite. To gain a better understanding of the carrier dynamics of the films, we performed time-resolved PL (TrPL) measurements of the films upon excitation at 480 nm (Figure 2b). The TrPL decay curves were fitted to a biexponential decay function (Table S1). All the THPPO-treated perovskite thin films exhibited significantly prolonged PL lifetimes for the fast and slow components of the PL decay (t1 and t2, respectively). For example, the film with 0.030 M THPPO had t1 = 19.0 ns and t2 = 192.3 ns, while the control film had t1 =12.6 ns and t2 = 96.4 ns, indicating that THPPO can effectively reduce the density of traps on the surface of the perovskites by passivation.

X-ray diffraction (XRD) of the perovskite films showed the typical pattern of the triple-cation and mixed-halide perovskites. 56 The deposition of THPPO did not cause an additional formation of a new pattern, indicating that it did not alter the crystalline structure of the perovskites (Figure 2c). As we used an excessive amount of PbI2 in the perovskite, the pristine film accordingly showed a noticeable peak at 12.7° that can be assigned to the residual PbI2. However, the peak intensity was reduced by the deposition of THPPO. As PbI2 is a well-known Lewis acid, the reduction of the PbI2 peak intensity of the THPPO-treated films can be explained by the formation of the PbI2·THPPO adduct (Figure 2c).57,58

The surface morphology of the perovskite films treated with various concentrations of THPPO was observed by scanning electron microscopy (SEM) images (Figure 3a). The pristine film showed sparsely distributed bright grains, which can be attributed to the residual PbI2. Upon the deposition of 0.005 M THPPO, the density of the bright grains decreased, and the color became darker as PbI2 was transformed into the PbI2·THPPO adduct, which is consistent with the result of XRD.57 The use of 0.010 M THPPO decreased the effective area of perovskite grains while increasing its occupation between the grains. Therefore, the surface contact area between the perovskite grains and THPPO was significantly increased, possibly leading to more effective passivation. However, a further increase in the concentration of THPPO resulted in thicker and nonhomogeneous coverage on top of the perovskite grains showing a stronger contrast. The crosssectional SEM images showed well-deposited electron-transporting layers (compact TiO2/mesoporous TiO2/SnO2) and the perovskite layer (~500 nm) and the top Au electrode.

However, the THPPO layer was not easily recognized due to its very low thickness (Figure S4).

The presence of THPPO on the perovskite surface was characterized by X-ray photoelectron spectroscopy (XPS). The C 1s spectrum of the control film exhibited two main peaks at 285.5 and 288.4 eV, which can be attributed to the C−C bond and the C□O bond, respectively (Figure 3b).16 The increase in the THPPO concentration resulted in a significant increase in the peak intensity of the C−C bond because the deposited THPPO has an increasing number of C−C bonds of three pentyl chains with tetrahydropyran ether. The peak of the C□O bond at 288.4 eV may have originated from the contamination of the perovskite upon exposure to the ambient air during the sample transfer for the measurement.59 The peak at 532.3 eV of the control film in the O 1s spectra, can be also attributed to the O□C bond formed by the surface oxidation (Figure 3c).60,61 The deposition of THPPO caused an appearance of an additional peak at 533.1 eV that arose from tetrahydropyran and ether of THPPO showing a significant increase in the intensity with the increase in the concentration of THPPO.62 In the P 2p spectra, we confirmed a peak that originated from the P□O bond of THPPO at 133.7 eV (Figure 3d).63,64

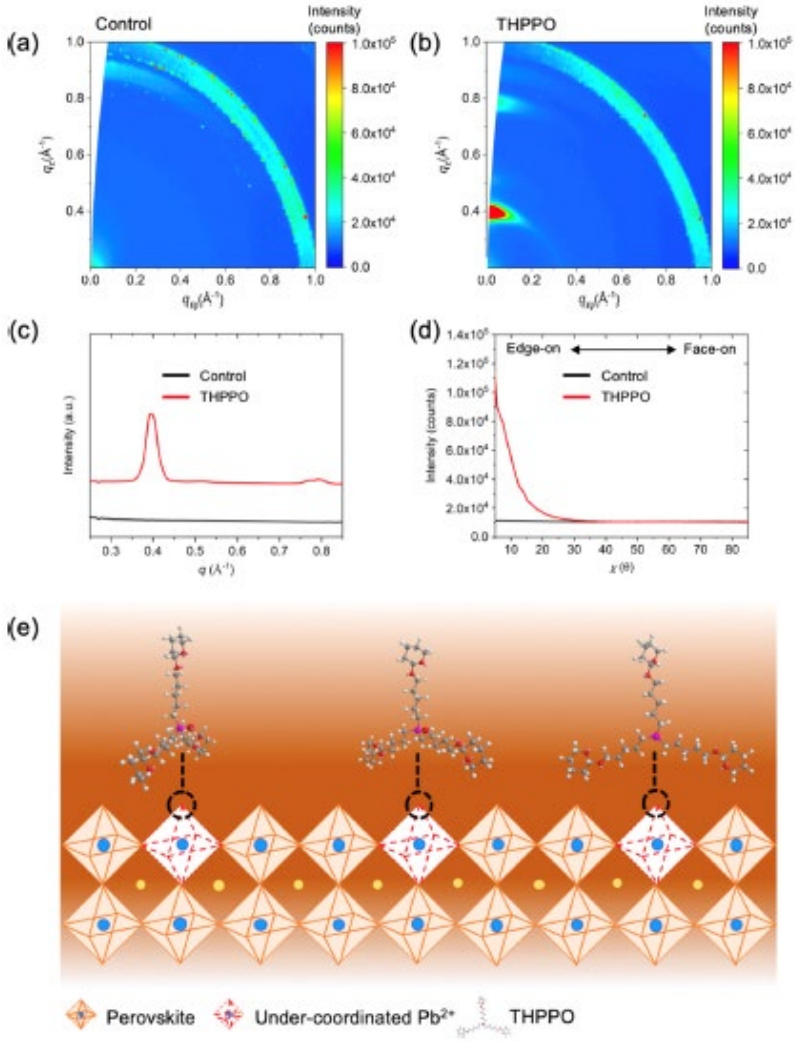

Figure 4. GIWAXS patterns of (a) control perovskite film and (b) THPPO-treated perovskite film. (c) Azimuthally integrated intensity profile obtained from GIWAXS patterns. (d) Angular dependence of the peak intensity at 0.40 Å−1. (e) Cartoon illustration of the proposed passivation mechanism. The concentration of THPPO is 0.030 M.

The Pb 4f spectra verified the passivation effect of THPPO (Figure 3e). The pristine film showed four prominent peaks at 136.9, 138.6, 141.8, and 143.4 eV. Pb 4f7/2 and Pb 4f5/2 peaks at 38.6 and 143.4 eV, respectively, can be attributed to lead halide bonds, while Pb 4f7/2 and Pb 4f5/2 peaks at 136.9 and 141.8 eV, respectively, can be attributed to Pb0. It is worth noting that the Pb0 peak can arise out of the undercoordinated Pb2+, which can act as a nonradiative recombination center, leading to the degradation of the device performance.65,66 Upon the deposition of THPPO, the apparent decrease in the intensity of Pb0 was observed and confirmed by the quantitative analysis of Pb0 (Table S2). The reduction in the Pb0 ratio can be explained by the coordination between the undercoordinated Pb2+ and the lone pair of electrons from the Lewis base of THPPO, which resulted in defect passivation. 40,67,68

To further elucidate the interaction between THPPO and the undercoordinated Pb2+ on the perovskite surface, we performed 31P NMR spectroscopy (Figure 3f). The measurement was carried out using 0.01 mmol THPPO dissolved in 0.5 mL of DMSO-d6, followed by the addition of 0.01 mmol PbI2. As the dissociation of PbI2 in the solution can yield the undercoordinated Pb2+, we can investigate the underlying mechanism of the passivation by examining its interaction with THPPO. While the phosphorous peak of pristine THPPO was at 46.76 ppm, the addition of PbI2 shifted the peak to 48.35

ppm. The downfield shift indicates that the electron density of the phosphorous nucleus decreases as the P□O functional group as a Lewis base donates electrons to Pb2+, triggering the passivation effect.42,43,45 To investigate the molecular stacking state of THPPO, we carried out grazing-incident wide-angle X-ray scattering (GIWAXS) analysis. The control film had a Debye−Scherrer ring at qz = 1.0 Å−1, which can be attributed to the (100) crystal planes of the cubic phase of the perovskite (Figure 4a).

Upon the deposition of THPPO on top of the perovskite layer, new peaks appeared at qz = 0.40 and 0.79 Å−1, which resulted from the out-of-plane orientation of THPPO on the perovskite layer (Figure 4b). Azimuthally integrated intensity profile of the film with THPPO also clearly showed the prominent peak at 0.40 Å−1 having a lattice spacing of 15.9 Å, which corresponds to the size of THPPO simulated by a molecular mechanics force field (Figures 4c and S5). The peak at 0.79Å−1 can be ascribed to the second diffraction peak of THPPO.

We examined the angular dependence of the diffraction peak at 0.40 Å−1 to obtain a detailed insight into the molecular stacking state of THPPO (Figure 4d). The intensity of the peak became prominently high at the low incident angle range below 20°, indicating a vertically well-aligned THPPO, socalled “edge-on” stacking. Therefore, the P□O group can effectively interact with the undercoordinated Pb2+ of the perovskite octahedral that can lead to the formation of the Lewis adduct, which agrees well with the result of the 31P NMR analysis.

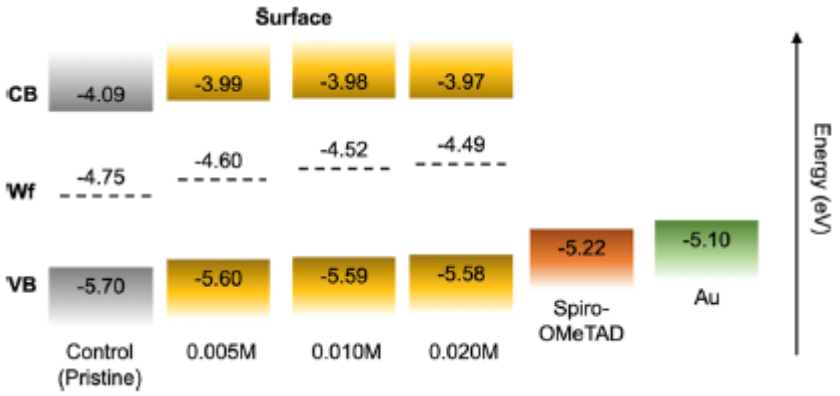

Figure 5. Energy-level diagram showing the valence band (VB), work function, and conduction band (CB) of the control and THPPOpassivated perovskite films.

performed ultraviolet photoelectron spectroscopy (UPS) to examine the energy-level alignment of perovskites upon the surface modification using THPPO (Figures 5 and S6). The control film exhibited a valence band (VB) energy of −5.70 eV and the energies gradually increased to −5.60, −5.59, and −5.58 eV according to the deposition of 0.005, 0.010, and 0.020 M of THPPO on top of the perovskite film, respectively. The positive shift in the VB edge by the THPPO treatment resulted in a favorable energetic alignment between perovskite and spiro-OMeTAD or gold electrode, which can facilitate hole transfer between the layers.

We employed THPPO as a passivating agent in PSCs without HTL (fluorine-doped tin oxide (FTO)/compact TiO2 (c-TiO2)/mesoporous TiO2 (mp-TiO2)/SnO2/perovskite/THPPO/Au). Various concentrations of THPPO from 0.005 to 0.030 M were applied to find an optimal condition of THPPO treatment in PSCs. All of the THPPO-passivated devices showed improved photovoltaic performance compared to the control device (Figure 6a and Table S3). The bestperforming device was achieved upon the deposition of 0.010 M THPPO having open-circuit voltage (VOC) of 0.866 V, short-circuit current density (JSC) of 23.32 mA cm−2, and fill factor (FF) of 0.689, resulting in a PCE of 13.31%. We also measured the external quantum efficiency (EQE) of the device (Figure S7). We statistically confirmed that the improvement of PCE by the THPPO treatment mainly resulted from the enhancement in VOC (Figure 6b and Table S4). The average VOC of the control device was 0.64 V and increased to 0.84 V with the use of 0.010 M of THPPO, and it saturated with further increase in the concentration of THPPO (Figure 6c).

The improvement in VOC can be ascribed to the reduced nonradiative recombination owing to the defect passivation effect of THPPO that we confirmed by the PL analyses.18 The average JSC and FF of the devices also improved by applying 0.010 M THPPO from 22.3 to 23.1 mA cm−2 and from 0.31 to 0.62, respectively. The improvements can be explained by the reduced density of trap states owing to the passivation effect of THPPO. In addition, the favorable energetic band alignment between THPPO and Au can lead to the facilitation of charge transfer. However, a further increase in the THPPO concentration degraded both JSC and FF because of the insulating nature of THPPO.49 It can hinder the efficient charge transfer by increasing the series resistance at the

interface (Figure S8 and Table S4). We also fabricated the device to compare THPPO and trioctylphosphine oxide (TOPO), one of the most widely used phosphine oxide based passivation agent.42,47,48 The device employing 0.010 M TOPO resulted in a lower photovoltaic performance with a PCE of 9.36% compared to that of the device using 0.010 M THPPO (Figure S9). Using the optimized THPPO treatment of 0.010 M, we developed PSCs including spiro-OMeTAD as an HTL (FTO/c-TiO2/mp-TiO2/SnO2/perovskite/THPPO/spiro-OMe-TAD/Au). Prior to the device fabrication, we performed 31P NMR spectroscopy to confirm the well-formed THPPO on top of the perovskite despite the deposition of spiro-OMeTAD, which also uses chlorobenzene as a solvent (Figure S10). While the control device exhibited VOC of 1.064 V, JSC of 23.76 mA cm−2, FF of 0.786, and PCE of 19.87%, the device with the THPPO passivation layer showed VOC of 1.108 V, JSC of 24.08 mA cm−2, FF of 0.776, and PCE of 20.70% (Figure 6d and Table S5). We measured the EQE spectrum of the device with passivation (Figure S11). Also, we evaluated the J−V hysteresis of the THPPO-passivated device and the control device by measuring them under reverse and forward bias scans. The control device showed PCEs of 19.85 and 17.70% under reverse and forward bias scans, respectively, resulting in a hysteresis index (HI) of 0.11 defined as

$$\frac{PCE_{reverse} - PCE_{forward}}{PCE_{reverse}}$$

Meanwhile, the THPPO-passivated device showed more stable J−V hysteresis behavior having HI of 0.06 resulted from the PCEs of 20.67 and 19.43% under reverse and forward bias scans, respectively (Figure S12). The improvement of the J−V characteristics can be attributed to the passivation effect and the favorable band alignment for charge extraction.

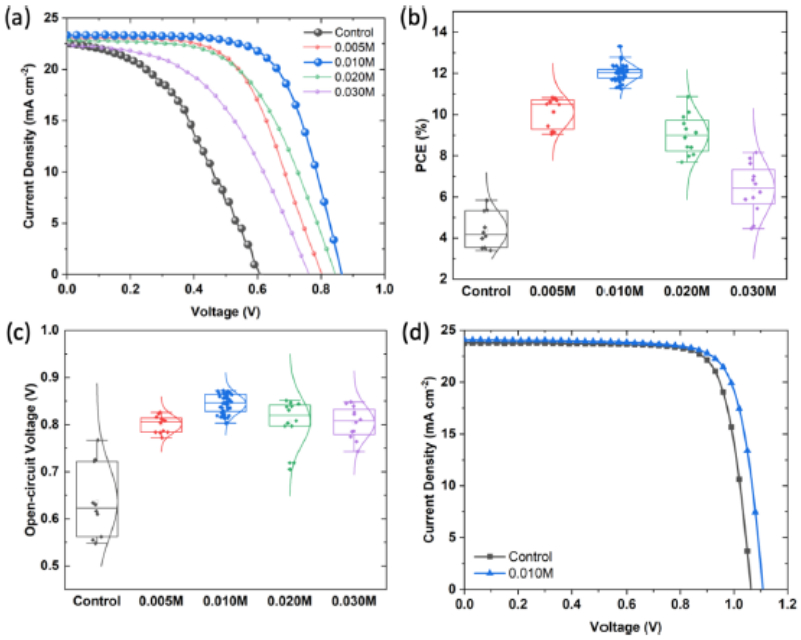

Lastly, we performed the stability measurement of the HTLfree devices by storing the devices under dark with the relative humidity kept below 10% (Figure S13). A significant improvement in the stability was observed for the THPPOpassivated device that retained 96% of its maximum efficiency after 360 h; however, the control device only retained 62% of its maximum efficiency for the same time window. The improvement in the device stability might be correlated with the THPPO's high decomposition temperature (Td) of 251 °C obtained from the thermogravimetric analysis (Figure S14).

CONCLUSIONS

We successfully synthesized a new molecule, THPPO, based on phosphine oxide derivative and demonstrated its application as a passivating agent in PSCs. We observed significant improvements in the PL characteristics of the perovskite films by introducing THPPO. It was attributed to the defect passivation effect of THPPO, which reduced the undesirable nonradiative recombination at the interface. Various analyses such as XPS, XRD, and 13P NMR spectroscopy verified the defect passivation effect in which a chemical interaction occurs between the undercoordinated Pb2+ and P□O functional group of THPPO. It can lead to the formation of the Lewis adduct based on the well-aligned THPPO on top of the perovskite layer. Consequently, the PCE of the HTL-free device increased from 5.84 to 13.31% and that of the device with spiro-OMeTAD as an HTL increased from 19.87 to 20.70%. We believe this study provides insights into an important approach to design a new passivating molecule that can improve the performance of the PSCs but also sheds light on the understanding of defect passivation mechanism.

EXPERIMENTAL SECTION

Fabrication of Perovskite Thin Films and Solar Cells. Fluorine-doped tin oxide coated glass (FTO, Nippon Sheet Glass) was used as the conducting electrode. Prior to each use, the FTO glass was patterned by chemical etching using Zn powder and aqueous HCl solution (3.0 M), then it was cleaned with detergent (Helmanex), deionized water, acetone, and isopropanol in an ultrasonic bath. A 30 nm thick compact TiO2 layer was used as the electron-transporting material and deposited on top of the FTO glass via spray pyrolysis of titanium diisopropoxide bis(acetylacetonate) (Sigma-Aldrich, diluted to 1:15 v/v in isopropanol) at 450 °C. A 100 nm thick mesoporous TiO2 layer was then deposited by spin-coating the ethanolic solution (1:8 v/v) of TiO2 paste (GreatCellSolar, 30NR-D) at 5000 rpm for 20 s, followed by heating at 10 min and sintering at 500 °C for 20 min. A 20 nm thick passivating tin oxide was spin-coated on top of a mesoporous TiO2 layer by dissolving tin(IV) chloride (Acros) solution (12 μL in 988 μL water) at 3000 rpm for 30 s, followed by annealing at 100 °C for 10 min and 190 °C for 1 h. UV-ozone treatment was carried out for 15 min before perovskite layer deposition. A triple-cation-based perovskite precursor solution [(FAPbI3)0.87(MAPbBr3)0.13]0.92(CsPbI3)0.08 with a concentration of 1.3 M was prepared by mixing formamidinium lead iodide (FAI) (GreatCellSolar), MABr (GreatCellSolar), CsI (ABCR), PbI2 (TCI), and PbBr2 (TCI) in

dimethylformamide (DMF) and DMSO (0.78:0.22 v/v). An excess concentration of PbI2 was used in the precursor solution (PbI2/FAI = 1.05:1). The perovskite solution was then deposited on top of the prepared substrates at 2000 rpm for 12 s and 5000 rpm for 30 s. Chlorobenzene was dropped at 15 s before the end of the spin-coating process. Perovskite film was annealed inside the glovebox for 60 min. Various concentrations of the THPPO solution (0.005, 0.010, 0.020, and 0.030 M) in chlorobenzene were deposited on top of the perovskite films at 4000 rpm for 30 s. For the HTL-based device, 2,2′,7,7′-tetrakis-(N,N-di-p-methoxyphenylamine)-9,9′-spirobifluorene (spiro-OMeTAD) is incorporated as the HTL. spiro-OMeTAD (Merck) with a concentration of 0.06 M dissolved chlorobenzene. One milliliter of the solution is doped with 18.57 μL of Li-bis(trifluoromethanesulphonyl)imide (Aldrich) from the stock solution (196 mg in 379 μL of acetonitrile), 13.69 μL of FK 209 Co(III) TFSI (GreatCellSolar) from the stock solution (99 mg in 263 μL of acetonitrile), and 31.28 μL of 4-tert-butylpyridine (Sigma-Aldrich). For a complete PSC device, a 70 nm thick gold counter electrode was deposited by physical vapor deposition under a highvacuum condition.

Device Characterization. The current density−voltage (J−V) characteristics were measured under xenon lamp solar simulator (450 W, Oriel Sol3A, AAA class). The light intensity was calibrated to 1 sun illumination using a Si reference equipped with an IR cutoff (KG5) filter. The J−V curves then recorded with a digital source meter (Keithley 2400) by applying an external voltage bias and measuring the current response. The active area was defined using a black metal mask with an aperture of 0.16 cm2. The J−V curves were scanned under the rate of 50 mV/s without any preconditioning. External quantum efficiency (EQE) spectra were recorded using IQE200B (Oriel). The long-term stability test was carried out under continuous 1 sun illumination and maximum power point (MPP) tracking with LED lamps in an inert (Ar) atmosphere without any encapsulation.

Thin-Film Characterization. *UV−vis Absorption*. The absorption spectra of the thin films were measured using an ultraviolet, visible, near-infrared spectrophotometer (PerkinElmer Lambda 950S).

Photoluminescence. Steady-state photoluminescence spectra of the perovskite thin films were measured using Fluorolog3-22 spectrofluorometer by exciting the films at 550 nm. Transient photoluminescence spectra were measured and recorded by a timecorrelated single-photon counting system (Nanofinder 30) at the excitation wavelength of 480 nm. The detection wavelength was set at 763−770 nm.

X-ray Diffraction (XRD). XRD measurements were performed on a Bruker D8 Advance diffractometer and non-monochromated Cu Kα radiation at ambient atmosphere and temperature.

Scanning Electron Microscopy (SEM). Cross-sectional and top surface SEM images were recorded by an in-lens detector of FEI Teneo scanning electron microscope at the accelerating voltage of 3 and 5 kV.

Grazing Incidence Wide-Angle X-ray Scattering (GIWAXS) Measurements. GIWAXS measurements were performed at SPring- 8 on beamline BL19B2. The X-ray irradiation with an energy of 12.39 keV (λ = 1 Å) was used on the sample at a fixed incident angle

on the order of 0.12° through a Huber diffractometer. A two-dimensional image detector (Pilatus 300 K) was used to record the 2D-GIWAXS patterns.

Ultraviolet Photoelectron Spectroscopy (UPS) Measurements. The ultraviolet photoelectron spectroscopy (UPS) was measured using a He−I source (hν = 21.22 eV) (AXIS Nova, Kratos Analytical Ltd., U.K.) to determine the valence band energy and the Fermi level. Gold (Au), which is in electrical contact with the sample, is used as a eference for the Fermi level of the samples.

X-ray Photoelectron Spectroscopy (XPS). The X-ray photoelectron spectroscopy (XPS) measurements were performed using VersaProbe II (Physical Electronics Inc) with a monochromator and Al Kα source of 1486.6 eV. The spectrum was referenced using the C−C bound component of the adventitious carbon.

ASSOCIATED CONTENT

Supporting Information: General information; general synthetic scheme; and synthetic methods and procedures along with Tables S1−S5 and Figures S1−S14 (PDF)

AUTHOR INFORMATION

Corresponding Authors

Hobeom Kim − Group for Molecular Engineering of Functional Materials, Institute of Chemical Sciences and Engineering, École Polytechnique Fédérale de Lausanne (EPFL), CH-1951 Sion, Switzerland; orcid.org/0000-0002-5296-8975; Email: hobeom.kim@epfl.ch

Mohammad Khaja Nazeeruddin − Group for Molecular Engineering of Functional Materials, Institute of Chemical Sciences and Engineering, École Polytechnique Fédérale de Lausanne (EPFL), CH-1951 Sion, Switzerland; orcid.org/0000-0001-5955-4786; Email: mdkhaja.nazeeruddin@epfl.ch

Authors

Albertus Adrian Sutanto − Group for Molecular Engineering of Functional Materials, Institute of Chemical Sciences and Engineering, École Polytechnique Fédérale de Lausanne (EPFL), CH-1951 Sion, Switzerland; orcid.org/0000-0002-9413-2789

Cansu Igci − Group for Molecular Engineering of Functional Materials, Institute of Chemical Sciences and Engineering, École Polytechnique Fédérale de Lausanne (EPFL), CH-1951 Sion, Switzerland

Hiroyuki Kanda − Group for Molecular Engineering of Functional Materials, Institute of Chemical Sciences and Engineering, École Polytechnique Fédérale de Lausanne (EPFL), CH-1951 Sion, Switzerland; orcid.org/0000-0002-0327-8775

Naoyuki Shibayama − Department of General Systems Studies, Graduate School of Arts and Sciences, The University of Tokyo, Tokyo 153-8904, Japan; orcid.org/0000-0003-2182-049X

Mounir Mensi − Institute of Chemical Sciences and Engineering, École Polytechnique Fédérale de Lausanne (EPFL), CH-1951 Sion, Switzerland

Valentin I. E. Queloz − Group for Molecular Engineering of Functional Materials, Institute of Chemical Sciences and Engineering, École Polytechnique Fédérale de Lausanne (EPFL), CH-1951 Sion, Switzerland

Cristina Momblona − Group for Molecular Engineering of Functional Materials, Institute of Chemical Sciences and Engineering, École Polytechnique Fédérale de Lausanne (EPFL), CH-1951 Sion, Switzerland; orcid.org/0000-0003-2953-3065

Hyung Joong Yun − Research Center for Materials Analysis, Korea Basic Science Institute, Daejeon 34133, Republic of Korea

Henk J. Bolink − Instituto de Ciencia Molecular, Universidad de Valencia, 46980 Paterna, Valencia, Spain; orcid.org/ 0000-0001-9784-6253

Aron J. Huckaba − Group for Molecular Engineering of Functional Materials, Institute of Chemical Sciences and Engineering, École Polytechnique Fédérale de Lausanne (EPFL), CH-1951 Sion, Switzerland

Author Contributions

A.A.S. and C.I. contributed equally to this work. A.A.S. fabricated and characterized the perovskite thin films and the solar cells. C.I. designed and synthesized the passivation molecule and characterized it. M.M. and H.J.Y. carried out the XPS experiments. Hiroyuki Kanda and N.S. performed TrPL, UPS, and GIWAXS measurements. V.I.E.Q. performed the steady-state PL measurement. C.M. assisted in the device preparation. A.A.S., C.I., and Hobeom Kim designed the experiments. Hobeom Kim and M.K.N. supervised the project. A.A.S., C.I., and Hobeom Kim wrote the manuscript with the contribution of the various authors for their parts. All authors

reviewed the manuscript.

Notes

The authors declare no competing financial interest.

ACKNOWLEDGMENTS

The authors acknowledge the Swiss National Science Foundation (SNSF) funding through the Synergia Grant EPISODE (Grant No. CRSII5_171000). The authors acknowledge funding from the European Commission's Horizon 2020 Research and Innovation Programme under Grant Agreement No. 763977 of the PerTPV project. The authors acknowledge Professor Raffaella Buonsanti for the useof the Fluorolog system. The authors thank Dr. Nakamura and

Dr. Koganezawa at the Japan Synchrotron Radiation Research Institute (JASRI). The GIWAXS measurement was performed at SPring-8 at BL19B2 with the approval of the JASRI, Proposal Nos. 2019B1807 and 2019B1808.

REFERENCES

(1) Best Research-Cell Efficiency Chart. https://www.nrel.gov/pv/cell-efficiency.html (accessed November 2020).

(2) Kojima, A.; Teshima, K.; Shirai, Y.; Miyasaka, T. Organometal Halide Perovskites as Visible-Light Sensitizers for Photovoltaic Cells. J. Am. Chem. Soc. 2009, 131, 6050−6051.

(3) Lin, Q.; Armin, A.; Nagiri, R. C. R.; Burn, P. L.; Meredith, P. Electro-Optics of Perovskite Solar Cells. Nat. Photonics 2015, 9, 106−112.

(4) Chen, Z.; Dong, Q.; Liu, Y.; Bao, C.; Fang, Y.; Lin, Y.; Tang, S.; Wang, Q.; Xiao, X.; Bai, Y.; Deng, Y.; Huang, J. Thin Single Crystal Perovskite Solar Cells to Harvest Below-bandgap Light Absorption. Nat. Commun. 2017, 8, No. 1890.

(5) Xing, G.; Mathews, N.; Lim, S. S.; Yantara, N.; Liu, X.; Sabba, D.; Grätzel, M.; Mhaisalkar, S.; Sum, T. C. Low-Temperature Solution-Processed Wavelength-Tunable Perovskites for Lasing. Nat. Mater. 2014, 13, 476−480.

(6) Huang, H.; Raith, J.; Kershaw, S. V.; Kalytchuk, S.; Tomanec, O.; Jing, L.; Susha, A. S.; Zboril, R.; Rogach, A. L. Growth Mechanism of Strongly Emitting CH3NH3PbBr3 Perovskite Nanocrystals with a Tunable Bandgap. Nat. Commun. 2017, 8, No. 996.

(7) Stranks, S. D.; Eperon, G. E.; Grancini, G.; Menelaou, C.; Alcocer, M. J. P.; Leijtens, T.; Herz, L. M.; Petrozza, A.; Snaith, H. J. Electron-Hole Diffusion Lengths Exceeding 1 Micrometer in an

Organometal Trihalide Perovskite Absorber. Science 2013, 342, 341−344.

(8) Xing, G.; Mathews, N.; Sun, S.; Lim, S. S.; Lam, Y. M.; Grätzel, M.; Mhaisalkar, S.; Sum, T. C. Long-Range Balanced Electron- and Hole-Transport Lengths in Organic-Inorganic CH3NH3PbI3. Science 2013, 342, 344−347.

(9) Dong, Q.; Fang, Y.; Shao, Y.; Mulligan, P.; Qiu, J.; Cao, L.; Huang, J. Electron-Hole Diffusion Lengths > 175 μm in Solution- Grown CH3NH3PbI3 Single Crystals. Science 2015, 347, 967−970.

(10) Savenije, T. J.; Ponseca, C. S.; Kunneman, L.; Abdellah, M.; Zheng, K.; Tian, Y.; Zhu, Q.; Canton, S. E.; Scheblykin, I. G.; Pullerits, T.; Yartsev, A.; Sundström, V. Thermally Activated Exciton Dissociation and Recombination Control the Carrier Dynamics in Organometal Halide Perovskite. J. Phys. Chem. Lett. 2014, 5, 2189−2194.

(11) Zhao, T.; Shi, W.; Xi, J.; Wang, D.; Shuai, Z. Intrinsic and Extrinsic Charge Transport in CH3NH3PbI3 Perovskites Predicted from First-Principles. Sci. Rep. 2016, 6, No. 19968.

(12) Kim, H.; Lim, K.-G.; Lee, T.-W. Planar Heterojunction Organometal Halide Perovskite Solar Cells: Roles of Interfacial Layers. Energy Environ. Sci. 2016, 9, 12−30.

(13) Correa-Baena, J.-P.; Tress, W.; Domanski, K.; Anaraki, E. H.; Turren-Cruz, S.-H.; Roose, B.; Boix, P. P.; Grätzel, M.; Saliba, M.; Abate, A.; Hagfeldt, A. Identifying and

Suppressing Interfacial Recombination to Achieve High Open-Circuit Voltage in Perovskite Solar Cells. Energy Environ. Sci. 2017, 10, 1207−1212.

(14) Schulz, P. Interface Design for Metal Halide Perovskite Solar Cells. ACS Energy Lett. 2018, 3, 1287−1293.

(15) Stolterfoht, M.; Wolff, C. M.; Márquez, J. A.; Zhang, S.; Hages, C. J.; Rothhardt, D.; Albrecht, S.; Burn, P. L.; Meredith, P.; Unold, T.; Neher, D. Visualization and Suppression of Interfacial Recombination for High-Efficiency Large-Area pin Perovskite Solar Cells. Nat. Energy 2018, 3, 847−854.

(16) Jiang, Q.; Zhao, Y.; Zhang, X.; Yang, X.; Chen, Y.; Chu, Z.; Ye, Q.; Li, X.; Yin, Z.; You, J. Surface Passivation of Perovskite Film for Efficient Solar Cells. Nat. Photonics 2019, 13, 460−466.

(17) Son, D.-Y.; Lee, J.-W.; Choi, Y. J.; Jang, I.-H.; Lee, S.; Yoo, P. J.; Shin, H.; Ahn, N.; Choi, M.; Kim, D.; Park, N.-G. Self-Formed Grain Boundary Healing Layer for Highly Efficient CH3NH3PbI3 Perovskite Solar Cells. Nat. Energy 2016, 1, No. 16081.

(18) Kanda, H.; Shibayama, N.; Huckaba, A. J.; Lee, Y.; Paek, S.; Klipfel, N.; Roldan-Carmona, C.; Queloz, V. I. E.; Grancini, G.; Zhang, Y.; Abuhelaiga, M.; Cho, K. T.; Li, M.; Mensi, M. D.; Kinge, S.; Nazeeruddin, M. K. Band-Bending Induced Passivation: High Performance and Stable Perovskite Solar Cells Using a Perhydropoly-(silazane) Precursor. Energy Environ. Sci. 2020, 13, 1222−1230.

(19) Chen, B.; Yang, M.; Priya, S.; Zhu, K. Origin of J−V Hysteresis in Perovskite Solar Cells. J. Phys. Chem. Lett. 2016, 7, 905−917.

(20) Akin, S.; Arora, N.; Zakeeruddin, S. M.; Grätzel, M.; Friend, R. H.; Dar, M. I. New Strategies for Defect Passivation in High-Efficiency Perovskite Solar Cells. Adv. Energy Mater. 2020, 10,No. 1903090.

(21) Zhou, H.; Chen, Q.; Li, G.; Luo, S.; Song, T.-b.; Duan, H.-S.; Hong, Z.; You, J.; Liu, Y.; Yang, Y. Interface Engineering of Highly Efficient Perovskite Solar Cells. Science 2014, 345, 542−546.

(22) Yang, S.; Wang, Y.; Liu, P.; Cheng, Y.-B.; Zhao, H. J.; Yang, H. G. Functionalization of Perovskite Thin Films with Moisture-Tolerant Molecules. Nat. Energy 2016, 1, No. 15016.

(23) Wu, B.; Nguyen, H. T.; Ku, Z.; Han, G.; Giovanni, D.; Mathews, N.; Fan, H. J.; Sum, T. C. Discerning the Surface and Bulk Recombination Kinetics of Organic−Inorganic Halide Perovskite Single Crystals. Adv. Energy Mater. 2016, 6, No. 1600551.

(24) Han, G. S.; Chung, H. S.; Kim, B. J.; Kim, D. H.; Lee, J. W.; Swain, B. S.; Mahmood, K.; Yoo, J. S.; Park, N.-G.; Lee, J. H.; Jung, H. S. Retarding Charge Recombination in Perovskite Solar Cells Using Ultrathin MgO-coated TiO2 Nanoparticulate Films. J. Mater. Chem. A 2015, 3, 9160−9164.

(25) Hu, Q.; Wu, J.; Jiang, C.; Liu, T.; Que, X.; Zhu, R.; Gong, Q. Engineering of Electron-Selective Contact for Perovskite Solar Cells with Efficiency Exceeding 15%. ACS Nano 2014, 8, 10161−10167.

(26) Han, F.; Luo, J.; Zhao, B.; Wan, Z.; Wang, R.; Jia, C. Cesium Iodide Interface Modification for High Efficiency, High Stability and Low Hysteresis Perovskite Solar Cells. Electrochim. Acta 2017, 236, 122−130.

(27) Zhang, J.; Hu, Z.; Huang, L.; Yue, G.; Liu, J.; Lu, X.; Hu, Z.; Shang, M.; Han, L.; Zhu, Y. Bifunctional Alkyl Chain Barriers for Efficient Perovskite Solar Cells. Chem. Commun. 2015, 51, 7047−7050.

(28) Yuan, D.-X.; Yuan, X.-D.; Xu, Q.-Y.; Xu, M.-F.; Shi, X.-B.; Wang, Z.-K.; Liao, L.-S. A Solution-processed Bathocuproine Cathode Interfacial Layer for High-performance Bromine−iodine Perovskite Solar Cells. Phys. Chem. Chem. Phys. 2015, 17, 26653−26658.

(29) Jiang, L.-L.; Cong, S.; Lou, Y.-H.; Yi, Q.-H.; Zhu, J.-T.; Ma, H.; Zou, G.-F. Interface Engineering Toward Enhanced Efficiency of Planar Perovskite Solar Cells. J. Mater. Chem. A 2016, 4, 217−222.

(30) Zuo, L.; Chen, Q.; De Marco, N.; Hsieh, Y.-T.; Chen, H.; Sun, P.; Chang, S.-Y.; Zhao, H.; Dong, S.; Yang, Y. Tailoring the Interfacial Chemical Interaction for High-Efficiency Perovskite Solar Cells. Nano Lett. 2017, 17, 269−275.

(31) Wojciechowski, K.; Stranks, S. D.; Abate, A.; Sadoughi, G.; Sadhanala, A.; Kopidakis, N.; Rumbles, G.; Li, C.-Z.; Friend, R. H.; Jen, A. K. Y.; Snaith, H. J. Heterojunction Modification for Highly Efficient Organic−Inorganic Perovskite Solar Cells. ACS Nano 2014, 8, 12701−12709.

(32) Liu, Z.; Li, S.; Wang, X.; Cui, Y.; Qin, Y.; Leng, S.; Xu, Y.-x.; Yao, K.; Huang, H. Interfacial Engineering of Front-Contact with Finely Tuned Polymer Interlayers for High-Performance Large-Area Flexible Perovskite Solar Cells. Nano Energy 2019, 62, 734−744.

(33) Salado, M.; Ramos, F. J.; Manzanares, V. M.; Gao, P.; Nazeeruddin, M. K.; Dyson, P. J.; Ahmad, S. Extending the Lifetime of Perovskite Solar Cells Using a Perfluorinated Dopant. Chem-SusChem 2016, 9, 2708−2714.

(34) Chang, J.; Lin, Z.; Zhu, H.; Isikgor, F. H.; Xu, Q.-H.; Zhang, C.; Hao, Y.; Ouyang, J. Enhancing the Photovoltaic Performance of Planar Heterojunction Perovskite Solar Cells by Doping the Perovskite Layer with Alkali Metal Ions. J. Mater. Chem. A 2016, 4, 16546−16552.

(35) Li, X.; Ibrahim Dar, M.; Yi, C.; Luo, J.; Tschumi, M.; Zakeeruddin, S. M.; Nazeeruddin, M. K.; Han, H.; Grätzel, M. Improved Performance and Stability of Perovskite Solar Cells by Crystal Crosslinking with Alkylphosphonic Acid ω-Ammonium Chlorides. Nat. Chem. 2015, 7, 703−711.

(36) Kim, H.; Lee, S.-U.; Lee, D. Y.; Paik, M. J.; Na, H.; Lee, J.; Seok, S. I. Optimal Interfacial Engineering with Different Length of Alkylammonium Halide for Efficient and Stable Perovskite Solar Cells. Adv. Energy Mater. 2019, 9, No. 1902740.

(37) Jung, E. H.; Jeon, N. J.; Park, E. Y.; Moon, C. S.; Shin, T. J.; Yang, T.-Y.; Noh, J. H.; Seo, J. Efficient, Stable and Scalable Perovskite Solar Cells Using Poly(3-hexylthiophene). Nature 2019,

567, 511−515.

(38) Sutanto, A. A.; Drigo, N.; Queloz, V. I. E.; Garcia-Benito, I.; Kirmani, A. R.; Richter, L. J.; Schouwink, P. A.; Cho, K. T.; Paek, S.; Nazeeruddin, M. K.; Grancini, G. Dynamical Evolution of the 2D/3D Interface: A Hidden Driver Behind Perovskite Solar Cell Instability. J. Mater. Chem. A 2020, 8, 2343−2348.

(39) Kim, H.; Pei, M.; Lee, Y.; Sutanto, A. A.; Paek, S.; Queloz, V. I. E.; Huckaba, A. J.; Cho, K. T.; Yun, H. J.; Yang, H.; Nazeeruddin, M. K. Self-Crystallized Multifunctional 2D Perovskite for Efficient and Stable Perovskite Solar Cells. Adv. Funct. Mater. 2020, 30, No. 1910620.

(40) Noel, N. K.; Abate, A.; Stranks, S. D.; Parrott, E. S.; Burlakov, V. M.; Goriely, A.; Snaith, H. J. Enhanced Photoluminescence and Solar Cell Performance via Lewis Base Passivation of Organic−Inorganic Lead Halide Perovskites. ACS Nano 2014, 8, 9815−9821.

(41) Lin, Y.; Shen, L.; Dai, J.; Deng, Y.; Wu, Y.; Bai, Y.; Zheng, X.; Wang, J.; Fang, Y.; Wei, H.; Ma, W.; Zeng, X. C.; Zhan, X.; Huang, J. π-Conjugated Lewis Base: Efficient Trap-Passivation and Charge-Extraction for Hybrid Perovskite Solar Cells. Adv. Mater. 2017, 29, No. 1604545.

(42) deQuilettes, D. W.; Koch, S.; Burke, S.; Paranji, R. K.; Shropshire, A. J.; Ziffer, M. E.; Ginger, D. S. Photoluminescence Lifetimes Exceeding 8 μs and Quantum Yields Exceeding 30% in Hybrid Perovskite Thin Films by Ligand Passivation. ACS Energy Lett. 2016, 1, 438−444.

(43) Almeida, G.; Ashton, O. J.; Goldoni, L.; Maggioni, D.; Petralanda, U.; Mishra, N.; Akkerman, Q. A.; Infante, I.; Snaith, H. J.; Manna, L. The Phosphine Oxide Route Toward Lead Halide Perovskite Nanocrystals. J. Am. Chem. Soc. 2018, 140, 14878−14886.

(44) Munson, K. T.; Grieco, C.; Kennehan, E. R.; Stewart, R. J.; Asbury, J. B. Time-Resolved Infrared Spectroscopy Directly Probes Free and Trapped Carriers in Organo-Halide Perovskites. ACS Energy Lett. 2017, 2, 651−658.

(45) Yang, Z.; Dou, J. J.; Kou, S.; Dang, J. L.; Ji, Y. Q.; Yang, G. J.; Wu, W. Q.; Kuang, D. B.; Wang, M. Q. Multifunctional Phosphorus-Containing Lewis Acid and Base Passivation Enabling Efficient and Moisture-Stable Perovskite Solar Cells. Adv. Funct. Mater. 2020, 30, No. 1910710.

(46) Yang, S.; Dai, J.; Yu, Z.; Shao, Y.; Zhou, Y.; Xiao, X.; Zeng, X. C.; Huang, J. Tailoring Passivation Molecular Structures for Extremely Small Open-Circuit Voltage Loss in Perovskite Solar Cells. J. Am. Chem. Soc. 2019, 141, 5781−5787.

(47) Palazon, F.; Pérez-del-Rey, D.; Marras, S.; Prato, M.; Sessolo, M.; Bolink, H. J.; Manna, L. Coating Evaporated MAPI Thin Films with Organic Molecules: Improved Stability at High Temperature and Implementation in High-Efficiency Solar Cells. ACS Energy Lett. 2018, 3, 835−839.

(48) Braly, I. L.; deQuilettes, D. W.; Pazos-Outón, L. M.; Burke, S.; Ziffer, M. E.; Ginger, D. S.; Hillhouse, H. W. Hybrid Perovskite Films Approaching the Radiative Limit with Over 90% Photoluminescence Quantum Efficiency. Nat. Photonics 2018, 12, 355−361.

(49) Ambroz, F.; Xu, W.; Gadipelli, S.; Brett, D. J. L.; Lin, C.-T.; Contini, C.; McLachlan, M. A.; Durrant, J. R.; Parkin, I. P.; Macdonald, T. J. Room Temperature Synthesis of Phosphine-Capped Lead Bromide Perovskite Nanocrystals Without Coordinating Solvents. Part. Part. Syst. Charact. 2020, 37, No. 1900391.

(50) McGrath, F.; Ghorpade, U. V.; Ryan, K. M. Synthesis and Dimensional Control of CsPbBr3 Perovskite Nanocrystals Using Phosphorous Based Ligands. J. Chem. Phys. 2020, 152, No. 174702.

(51) Torres, A.; Rego, L. G. C. Surface Effects and Adsorption of Methoxy Anchors on Hybrid Lead Iodide Perovskites: Insights for Spiro-MeOTAD Attachment. J. Phys. Chem. C 2014, 118, 26947−26954.

(52) Cheng, H.-Y.; Sun, C.-S.; Hou, D.-R. Regioselective Palladium-Catalyzed Formate Reduction of N-Heterocyclic Allylic Acetates. J. Org. Chem. 2007, 72, 2674−2677.

(53) Zhang, Q.; Dong, J.; Meng, Q.; Huang, G.; Li, S. Synthesis and Cytotoxicity of 1,4-Naphthoquinone Oxime Derivatives. Russ. J. Gen. Chem. 2018, 88, 2388−2393.

(54) Behm, K.; Essner, J. B.; Barnes, C. L.; Baker, G. A.; Walensky, J. R. Synthesis and Fluorescence Spectroscopy of Tris(pyrenyl)-pnictogen Compounds. Dalton Trans. 2017, 46, 10867−10875.

(55) Zhang, J.-A.; Yang, N.-F.; Yang, L.-W.; Wu, S.; Chen, Y.-H.; Zhang, J. Synthesis of Chiral Bisacylphosphine Oxides and Their Application as Initiators in Helix-Sense-Selective Photopolymerization. Macromol. Res. 2013, 21, 641−648.

(56) Saliba, M.; Matsui, T.; Seo, J.-Y.; Domanski, K.; Correa-Baena, J.-P.; Nazeeruddin, M. K.; Zakeeruddin, S. M.; Tress, W.; Abate, A.; Hagfeldt, A.; Grätzel, M. Cesium-Containing Triple Cation Perovskite Solar Cells: Improved Stability, Reproducibility and High Efficiency. Energy Environ. Sci. 2016, 9, 1989−1997.

(57) Lim, K.-S.; Lee, D.-K.; Lee, J.-W.; Park, N.-G. 17% Efficient Perovskite Solar Mini-Module via Hexamethylphosphoramide (HMPA)-Adduct-Based Large-Area D-bar Coating. J. Mater. Chem. A 2020, 8, 9345−9354.

(58) Sun, K.; Hu, Z.; Shen, B.; Lu, C.; Huang, L.; Zhang, J.; Zhang, J.; Zhu, Y. Lewis Acid−Base Interaction-Induced Porous PbI2 Film for Efficient Planar Perovskite Solar Cells. ACS Appl. Energy Mater. 2018, 1, 2114−2122.

(59) Chen, P.; Bai, Y.; Wang, S.; Lyu, M.; Yun, J.-H.; Wang, L. In Situ Growth of 2D Perovskite Capping Layer for Stable and Efficient Perovskite Solar Cells. Adv. Funct. Mater. 2018, 28, No. 1706923.

(60) Wang, D. H.; Hu, Y.; Zhao, J. J.; Zeng, L. L.; Tao, X. M.; Chen, W. Holey Reduced Graphene Oxide Nanosheets for High Performance Room Temperature Gas Sensing. J. Mater. Chem. A 2014, 2, 17415−17420.

(61) Rocks, C.; Svrcek, V.; Maguire, P.; Mariotti, D. Understanding Surface Chemistry During MAPbI3 spray deposition and its effect on photovoltaic performance. J. Mater. Chem. C 2017, 5, 902−916.

(62) Dong, S.-S.; Shao, W.-Z.; Yang, L.; Ye, H.-J.; Zhen, L. Surface Characterization and Degradation Behavior of Polyimide Films Induced by Coupling Irradiation Treatment. RSC Adv. 2018, 8, 28152−28160.

(63) Yerushalmi, R.; Ho, J. C.; Fan, Z.; Javey, A. Phosphine Oxide Monolayers on SiO2 Surfaces. Angew. Chem., Int. Ed. 2008, 47, 4440−4442.

(64) Biagiotti, G.; Langè, V.; Ligi, C.; Caporali, S.; Muniz-Miranda, M.; Flis, A.; Pietrusiewicz, K. M.; Ghini, G.; Brandi, A.; Cicchi, S. Nanostructured Carbon Materials Decorated with Organophosphorus Moieties: Synthesis and Application. Beilstein J. Nanotechnol. 2017, 8, 485−493.

(65) Yang, Y.; Wu, J.; Wang, X.; Guo, Q.; Liu, X.; Sun, W.; Wei, Y.; Huang, Y.; Lan, Z.; Huang, M.; Lin, J.; Chen, H.; Wei, Z. Suppressing Vacancy Defects and Grain Boundaries via Ostwald Ripening for High-Performance and Stable Perovskite Solar Cells. Adv. Mater. 2020, 32, No. 1904347.

(66) Wang, L.; Zhou, H.; Hu, J.; Huang, B.; Sun, M.; Dong, B.; Zheng, G.; Huang, Y.; Chen, Y.; Li, L.; Xu, Z.; Li, N.; Liu, Z.; Chen, Q.; Sun, L.-D.; Yan, C.-H. A Eu3+-Eu2+ Ion Redox Shuttle Imparts Operational Durability to Pb-I Perovskite Solar Cells. Science 2019, 363, 265−270.

(67) Zhang, W.; Pathak, S.; Sakai, N.; Stergiopoulos, T.; Nayak, P. K.; Noel, N. K.; Haghighirad, A. A.; Burlakov, V. M.; deQuilettes, D. W.; Sadhanala, A.; Li, W.; Wang, L.; Ginger, D. S.; Friend, R. H.; Snaith, H. J. Enhanced Optoelectronic Quality of Perovskite Thin Films with Hypophosphorous Acid for Planar Heterojunction Solar Cells. Nat. Commun. 2015, 6, No. 10030.

(68) Lindblad, R.; Bi, D.; Park, B.-w.; Oscarsson, J.; Gorgoi, M.; Siegbahn, H.; Odelius, M.; Johansson, E. M. J.; Rensmo, H. Electronic Structure of TiO2/CH3NH3PbI3 Perovskite Solar Cell Interfaces. J. Phys. Chem. Lett. 2014, 5, 648−653.